J. Fluid Mech. (1990), *vol.* 214, *pp.* 395–410
Printed in Great Britain

An analytic model of sound production by raindrops

By MICHAEL S. LONGUET-HIGGINS
Center for Studies of Nonlinear Dynamics, La Jolla Institute, 7855 Fay Avenue, Suite 320, La Jolla, CA 92037, USA

(Received 28 June 1989 and in revised form 5 October 1989)

Observations of the cavity produced by a droplet of rain falling on a plane water surface show that the cavity often takes the form of an inverted cone. In the present paper we discuss a simple analytic expression for the corresponding fluid flow.

The main source of rain noise has been found to occur when the flow entrains an air bubble at the vertex of the cone. In this paper we show that the magnitude of the sound produced by the fluid flow in the present model is consistent with observation.

1. Introduction

Striking progress has recently been made in understanding the spectrum of underwater sound due to rain. Extending the earlier studies by Wenz (1962) and others to frequencies above 10 kHz, Scrimger (1985) and Nystuen (1986) found a characteristic peak in the spectrum at about 15 kHz, a result well confirmed by the recent work of Scrimger *et al.* (1987, 1989) and by Pumphrey, Crum & Bjorno (1989). At the same time, laboratory experiments by Pumphrey & Crum (1988, 1989) on the vertical impact of water droplets on a plain water surface have demonstrated that most of the sound arises not from the initial impact itself but from bubbles entrained near the bottom of the resulting surface cavity. For any given initial drop size, such 'regular entrainment' occurs only rather exceptionally, namely when the impact velocity lies in a certain narrow range. These observations have been beautifully confirmed by the numerical calculations of Oguz & Prosperetti (1989*a*); see also Prosperetti, Crum & Pumphrey (1989).

Intriguingly, the surface profile of the impact cavity (according to both laboratory experiments and numerical calculations) often assumes the form of an inverted cone; see figures 1 to 5 below. In figure 1, for example, a bubble is ultimately enclosed. In figure 2(*a*), a bubble is also formed, but in figures 2(*b*) and 2(*c*) the impact velocity was too high. Similarly in figure 3 the velocity was too low to enclose a bubble, but in figures 4 and 5 a bubble is again enclosed. In each case the outer surface of the bubble cavity is roughly conical. It therefore seems worthwhile to inquire whether there are any simple flows, given analytically, in which the profile can assume a conical form; and if so, whether such a model can be used to make a direct estimate of the resulting emitted sound.

In §§2–4 of this paper we treat the outer part of the cavity, where surface tension may be negligible, and show that there is indeed such a simple flow. In fact it is one of a class of hyperbolic flows found previously, which describe the jets formed by the disintegration of a bubble film (see Longuet-Higgins 1983). Analytically, it is a simple, linear shear, described by a spherical harmonic of degree 2. The time dependence develops a singularity at the instant when the vertex angle of the conical

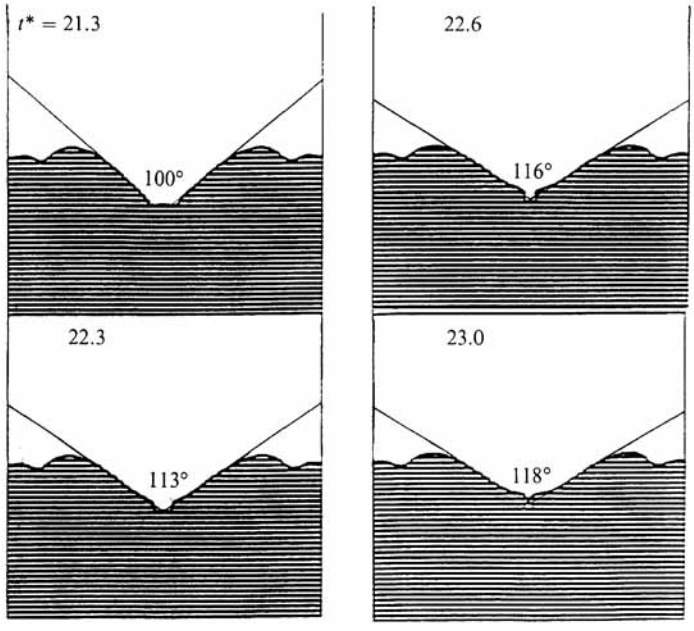

FIGURE 1. Axial section of the cavity from a drop of radius $R = 1.9$ mm and impact velocity $U = 1.53$ m/s. The times indicated are in the dimensionless units R/U (after Oguz & Prosperetti 1989*a*).

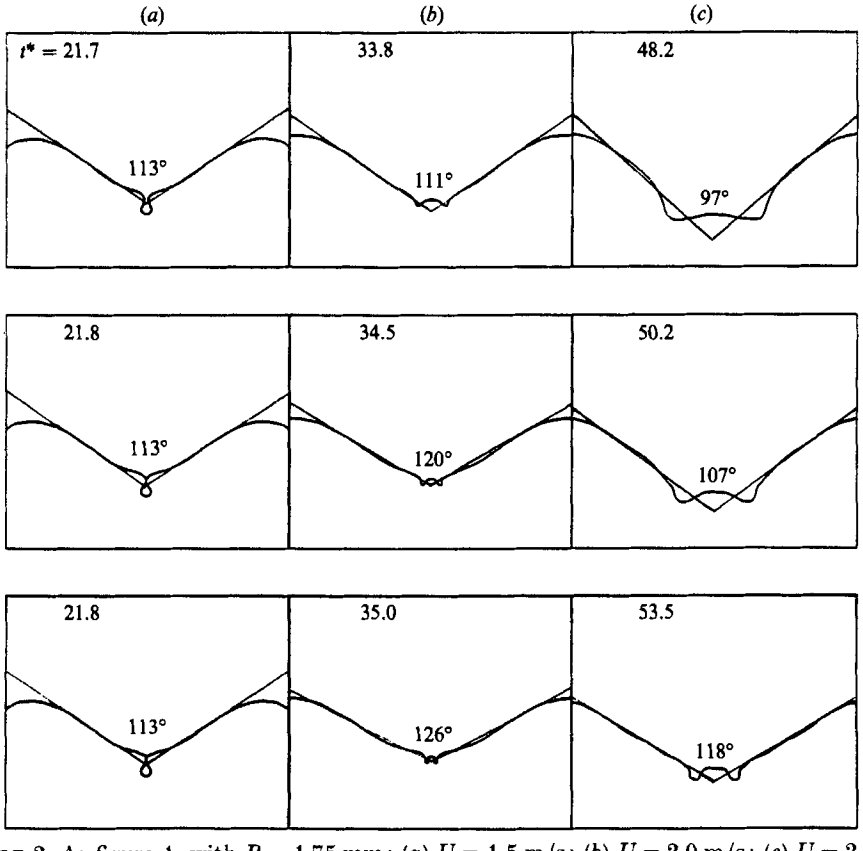

FIGURE 2. As figure 1, with $R = 1.75$ mm: (*a*) $U = 1.5$ m/s; (*b*) $U = 2.0$ m/s; (*c*) $U = 2.5$ m/s.

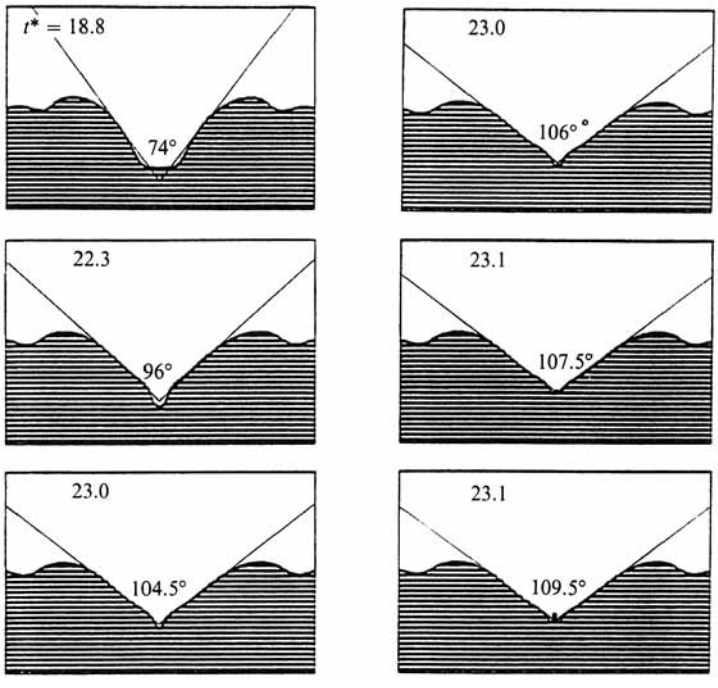

FIGURE 3. As figure 1, with $R = 1$ mm, $U = 1.75$ m/s.

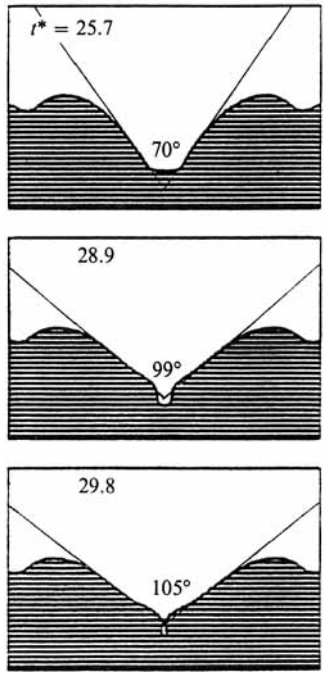

FIGURE 4. As figure 1, with $R = 1$ mm, $U = 2.0$ m/s.

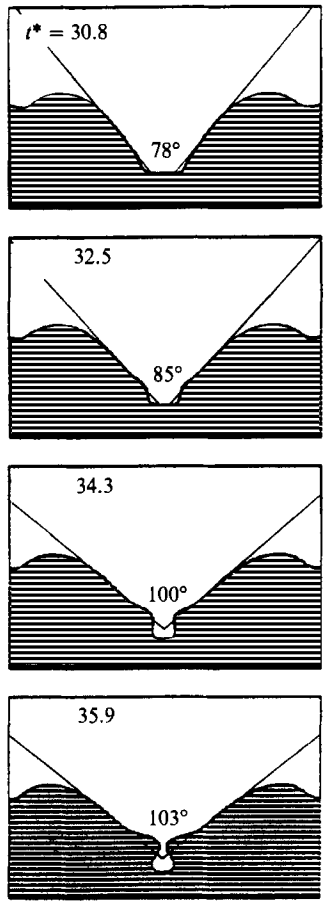

FIGURE 5. As figure 1, with $R = 1$ mm, $U = 2.4$ m/s.

boundary passes through the critical angle 109.5°. Comparison with the experimental data shows some agreement with the observed vertex angle. Moreover, the time dependence of the vertex angle appears to behave in the manner predicted.

In §5 it is shown that surface tension may be included by placing at the vertex of the cone a simple sink, whose strength varies linearly with the time.

The development of the bubble cavity, which arises from a circular ripple converging on the vertex, is discussed in §6. In §7 we calculate the strength of the sound pulse, and conclusions follow in §8.

2. Equations for the outer cavity

Since the wavelength of sound is large compared with the lengthscale of the cavity, we assume the motion to be incompressible. Further, since there is little time for the diffusion of vorticity, the motion is assumed irrotational. Hence there is a velocity potential ϕ satisfying

$$\nabla^2\phi = 0 \tag{2.1}$$

in the interior. Taking the density as unity, we have also the Bernoulli equation

$$p + \tfrac{1}{2}(\nabla\phi)^2 + gz + \phi_t = 0, \tag{2.2}$$

where z is a vertical coordinate, measured upwards and g denotes gravity. Because of the large particle accelerations involved (of order 10^4 cm/s^2 or more) we may take $g = 0$. Hence

$$p = -\phi_t - \tfrac{1}{2}(\nabla\phi)^2. \tag{2.3}$$

In the outer part of the cavity we shall ignore surface tension, so that the dynamical boundary condition is simply

$$p = 0. \tag{2.4}$$

To this we must joint the kinematic boundary condition, expressible as

$$\left(\frac{\partial}{\partial t} + \nabla\phi\cdot\nabla\right)p = 0. \tag{2.5}$$

3. A simple instantaneous flow

Axisymmetric solutions to Laplace's equation (2.1) exist in the form

$$\phi = Ar^n P_n(\cos\theta), \tag{3.1}$$

where r and θ are spherical coordinates as shown in figure 6, and A is a function of the time t only. In particular when $n = 2$ and $A(t) = t$ we have

$$\phi = \tfrac{1}{2}tr^2(3\cos^2\theta - 1). \tag{3.2}$$

At time $t = 0$ it is clear that $\nabla\phi$ vanishes and so by (2.3)

$$p = -\tfrac{1}{2}r^2(3\cos^2\theta - 1) \tag{3.3}$$

which vanishes when $\cos^2\theta = \frac{1}{3}$, that is

$$\theta = \arccos 3^{-\frac{1}{2}} = 54.7^\circ = \theta_c \tag{3.4}$$

say, hence the instantaneous free surface is a cone with vertex angle

$$2\gamma_c = 109.5^\circ \tag{3.5}$$

4. An exact conical flow

The simple flow given by (3.2) does not satisfy the boundary condition (2.4) at times other than $t = 0$, nor does it generally satisfy the condition (2.5). At times $t \neq 0$, further terms must be included in the solution, and the free surface will no longer be conical.

Remarkably, however, there does exist an exact, axisymmetric solution to the boundary condition (2.6) and (2.5) having the form

$$\phi = \tfrac{1}{2}A(t)\,r^2(3\cos^2\theta - 1) \tag{4.1}$$

and in which the free surface is always a cone. This solution is in fact a special case of one of the hyperbolic flows discussed by the author in an earlier paper (Longuet-Higgins 1983).

Note first that when expressed in terms of Cartesian coordinates (x, y, z) with the origin at the vertex and x vertically upwards, (4.1) becomes

$$\phi = \tfrac{1}{2}A(2z^2 - x^2 - y^2). \tag{4.2}$$

The velocity vector

$$\nabla\phi = A(-x, -y, 2z) \tag{4.3}$$

depends linearly on x, y and z. Hence any material particles lying in a straight line

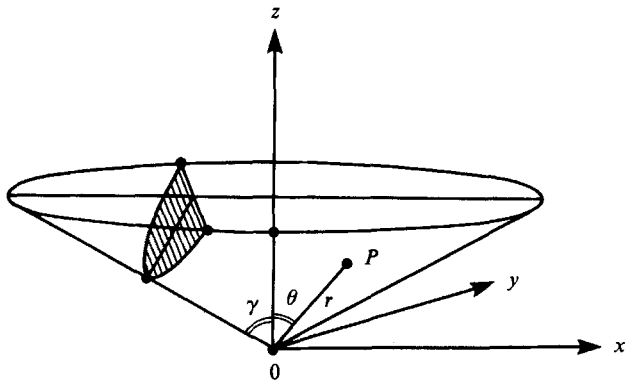

FIGURE 6. Definition of coordinates.

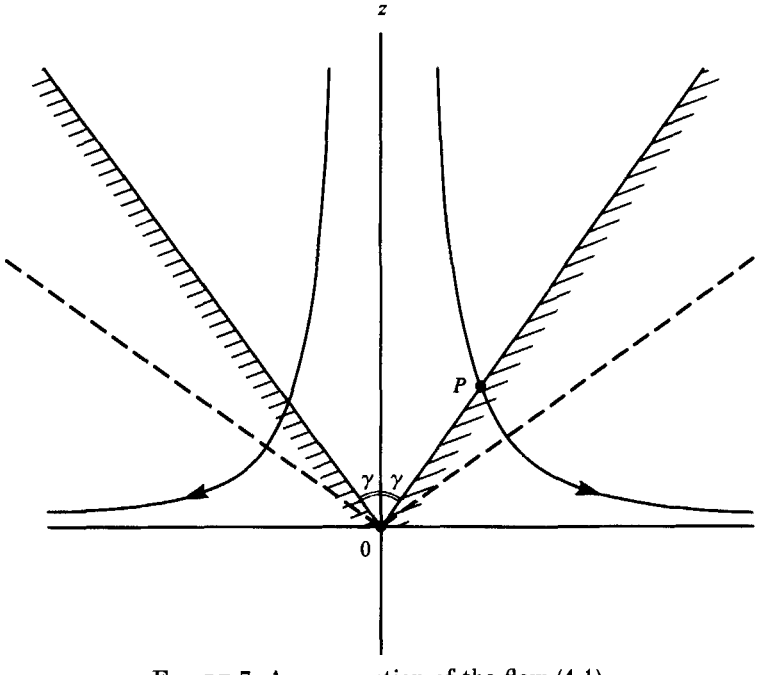

FIGURE 7. A cross-section of the flow (4.1).

remain always in a straight line, although the direction of the line generally varies in time. Thus, particles on the surface of a cone remain always on the surface of a cone, although the vertex angle 2γ depends on the time t (see figure 7).

Figure 7 shows how the trajectory of a typical particle always curves away from the axis of symmetry. To produce such a curvature there must clearly be a component of the pressure gradient normal to the trajectory. Consider then a typical point P on the free surface. Since the component of the pressure gradient parallel to the free surface vanishes, the gradient is always normal to the surface. At a general angle, the pressure gradient can supply a component of force normal to the trajectory, but at a certain critical angle this becomes impossible, namely when

$$(x, y, z) \cdot \nabla\phi = 0 \tag{4.4}$$

or from (4.3)

$$x^2 + y^2 - 2z^2 = 0, \tag{4.5}$$

hence
$$3\cos^2\theta - 1 = 0. \tag{4.6}$$

This makes the vertex angle of the cone 109.5° as before. At this critical angle, if the free surface is to remain conical, the flow must have a singularity in time. Physically, it appears difficult to force the flow past the critical configuration.

Does this fit the observations? In figures 1 to 5 we have drawn straight lines approximately tangent to the free surface in the outer part of each cavity. Thus in figure 1 the vertex angle is stationary at around 118°. In figure 2 the maximum angles are 113°, 126° and 118°, only the first one forming a bubble. In figures 3, 4 and 5 the maximum angles are 109.5°, 105° and 103°. The mean value of all these angles is 113°. The agreement with equation (4.6) is encouraging.

A derivation of the actual time dependence is given in Longuet-Higgins (1983). It is found that $A(t)$ can be expressed in the form

$$A = \frac{\dot{\lambda}}{2\lambda} \quad \left(\dot{} = \frac{\mathrm{d}}{\mathrm{d}t}\right) \tag{4.7}$$

where λ is given in terms of the time t by the elliptic integral

$$\frac{t}{t_0} = \pm \int_1^{\lambda} (1-\lambda^{-3})^{\frac{1}{2}} \mathrm{d}\lambda, \tag{4.8}$$

t_0 being an arbitrary constant. The pressure p is given by

$$p = \frac{\ddot{\lambda}}{4\lambda}[\lambda^3(x^2+y^2-2z^2)]. \tag{4.9}$$

Thus the free surface $p = 0$ is a cone with semi-vertex angle

$$\gamma = \arctan\,(2/\lambda^3)^{\frac{1}{3}}. \tag{4.10}$$

The time dependence of γ is shown in figure 8. The singularity when $\lambda = 1$, $2\gamma = 109.5°$, can be seen.

Close to the critical time $t = 0$, which corresponds to $\lambda = 1$, we find from (4.9) that

$$\lambda \approx 1 + \tau^{\frac{2}{3}}, \quad \tau = -\frac{3^{\frac{1}{3}}}{2}\frac{t}{t_0}, \tag{4.11}$$

so that the velocity field, which is proportional to $\dot{\lambda}/\lambda$, becomes weakly infinite like $|t|^{-\frac{1}{3}}$, and the pressure field becomes infinite like $|t|^{-\frac{2}{3}}$. Near $t = 0$ we find from (4.10) and (4.11) that

$$\tan\gamma \approx 2^{\frac{1}{3}}(1-\tfrac{3}{2}\tau^{\frac{3}{2}}). \tag{4.12}$$

Hence, the departure

$$\Delta\gamma = \arctan 2^{\frac{1}{3}} - \gamma \tag{4.13}$$

of the vertex angle from its limiting value is proportional to $|t^{\frac{2}{3}}|$.

In figure 9 we have plotted $(2\Delta\gamma)^{\frac{2}{3}}$ against the dimensionless time τ. The full curve is taken from the calculated values in table 1 of Longuet-Higgins (1983). The broken line corresponds to the $\tau^{\frac{3}{2}}$ asymptote. The gradient of the line is $3^{\frac{1}{3}}/2^{\frac{1}{3}} = 1.456$.

To test this time-dependence we measured the vertex angles 2γ from figure 4 above (Oguz & Prosperetti 1989*a*, figure 11*c*).† Some intermediate surface profiles with

† The angles were determined by tangents such that each touched the outer part of the profile, and divided the line joining the maximum and minimum nearest the axis of symmetry in the ratio 5:2; see §6 below.

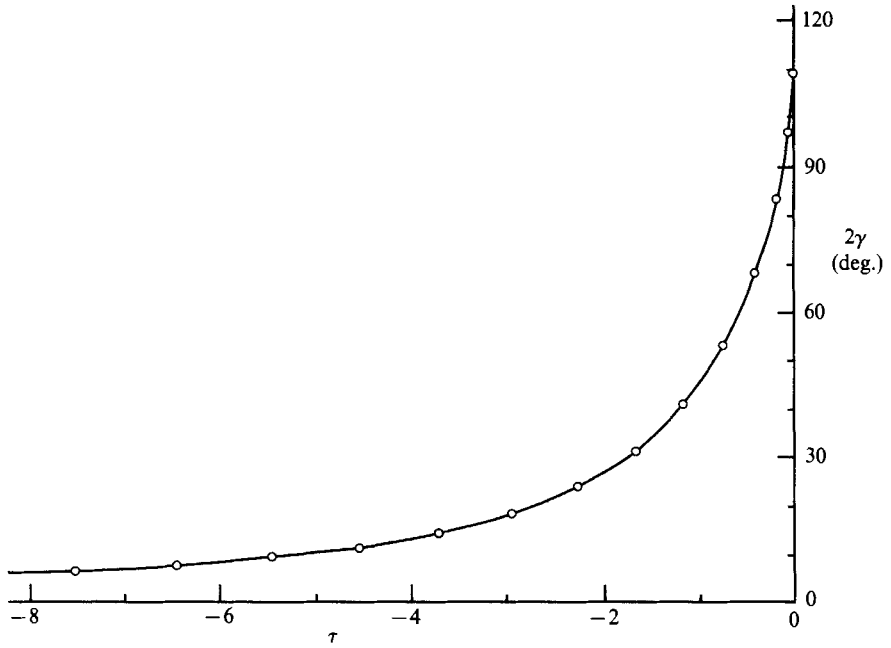

FIGURE 8. Time-dependence of the vertex angle 2γ in the flow (4.1).

more accurate timing were very kindly supplied by Dr H. Oguz. In figure 10 we have plotted $(2\Delta\gamma)^{\frac{3}{2}}$ versus the dimensionless time t^* used by Oguz & Prosperetti, and it will be seen that the observed points follow the theoretical curve rather well. The intercept of the line with the horizontal axis at $t^* = 23.45$ may be taken as the origin of time for the conical flow.

A second example, which corresponds more closely to a typical raindrop at terminal velocity, is illustrated in figure 11. The corresponding analysis of $\Delta\gamma$ is shown in figure 12. Again the plotted points lie well along the theoretical curve.

5. Surface tension

So far we have ignored surface tension. Generally, the effect of surface tension is to reduce the pressure p in the fluid just inside the boundary by an amount

$$p' = -T(\kappa_1 + \kappa_2) \tag{5.1}$$

where κ_1 and κ_2 denote the principal curvatures. In the case of a cone with vertex angle 2γ we have

$$\kappa_1 = 0, \quad \kappa_2 = \frac{1}{r}\cot\gamma, \tag{5.2}$$

r being the radial distance, and the pressure just inside the boundary must therefore be

$$p = -\frac{T\cot\gamma}{r}. \tag{5.3}$$

When the velocity is small, this is precisely the pressure field induced by a sink

$$\phi' = \frac{T/\rho}{r} f(t), \tag{5.4}$$

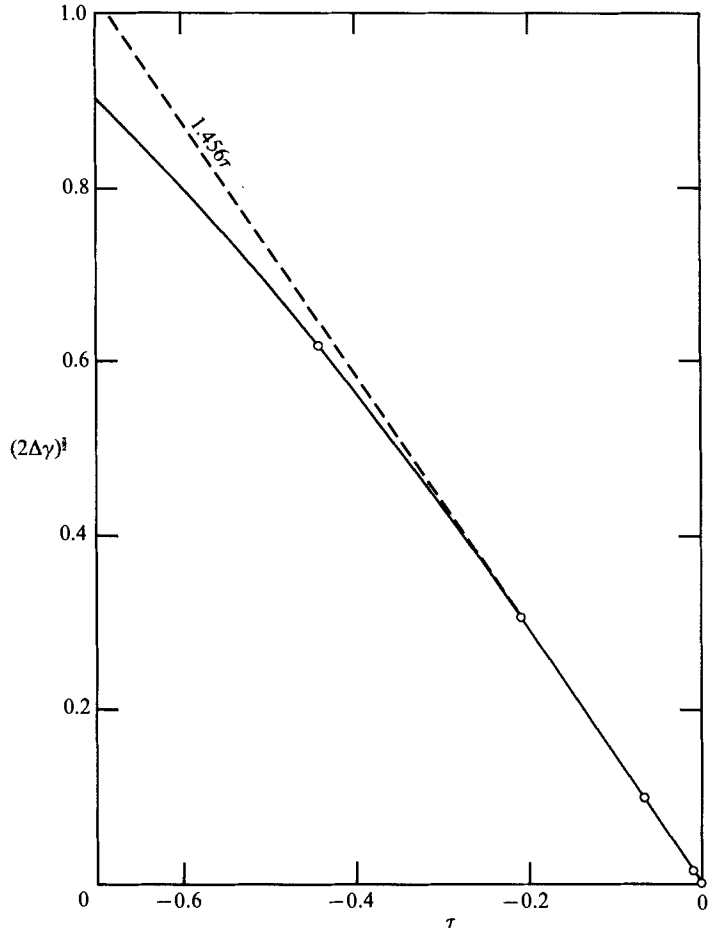

FIGURE 9. Graph showing the behaviour of the vertex angle 2γ in the neighbourhood of the critical instant $t = 0$. Full curve represents $(2\Delta\gamma)^{\frac{3}{2}}$, from calculated values in table 1 of Longuet-Higgins (1983). Broken line represents linear asymptote.

where ρ denotes the density, provided that

$$\frac{\mathrm{d}f}{\mathrm{d}t} = \cot\gamma. \tag{5.5}$$

From (4.6) we have

$$\cot\gamma = \frac{1}{2^{\frac{1}{2}}} + O(\tau^{\frac{2}{3}}), \tag{5.6}$$

hence

$$\phi' \sim \frac{T/\rho}{2^{\frac{1}{2}}} \frac{t}{r}. \tag{5.7}$$

We can imagine this sink placed in the cavity that appears, experimentally, near the vertex of the cone, just before the bubble breaks away.

The solution combining both (4.1) and (5.7) does not in fact satisfy the boundary condition exactly, on account of the nonlinearity of the pressure condition. Nevertheless it may describe approximately the actual velocity field.

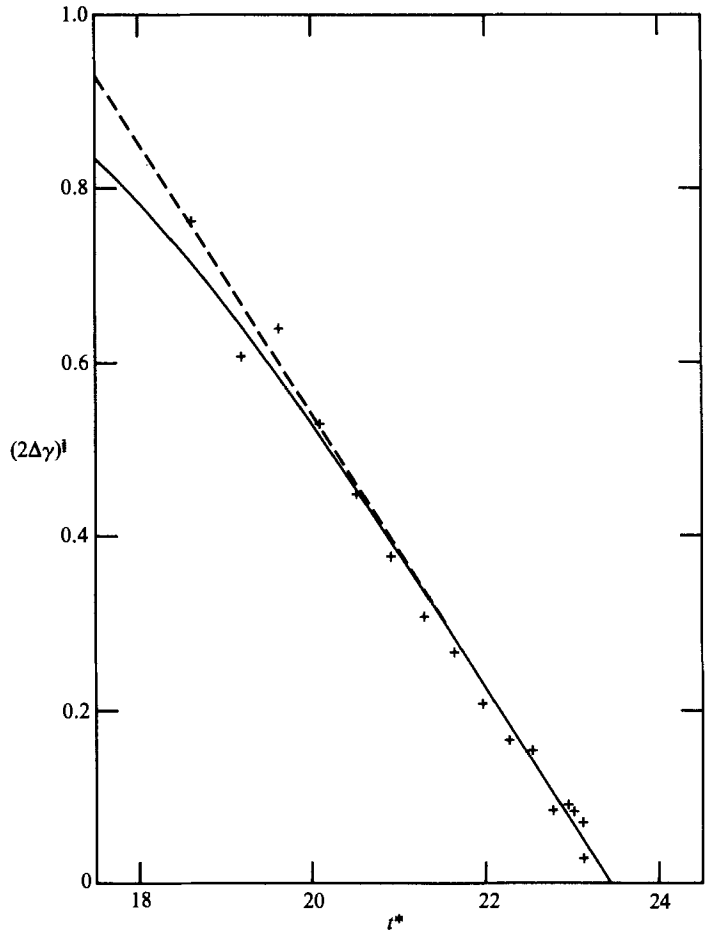

FIGURE 10. A plot of $(2\Delta\gamma)^{\frac{1}{2}}$ versus the dimensionless time t^* corresponding to figure 3 (Oguz & Prosperetti 1989*a*). figure 11*c*), $U = 1.75$ m/s, $R = 1$ mm.

6. Development of the bubble cavity

In both the experiments and numerical computations the cavity at the vertex seems to arise out of a ripple on the surface of the cone converging towards the axis of symmetry. This convergent ripple may be considered as a perturbation of the conical flow on a relatively small (capillary) lengthscale. Qualitatively, the behaviour of the 'ripple' will not differ greatly from the inward propagation of a circular ripple on a plane water surface. Accordingly near the time of arrival of the ripple energy at the axis of symmetry, the surface displacement η will be described roughly by the Bessel function J_0:

$$\eta \propto J_0(kr)\,e^{i\sigma t}, \quad \sigma^2 = (T/\rho)\,k^3, \tag{6.1}$$

where k is a local wavenumber. We note that the ratio of the first maximum of J_0 ($J_0(0) = 1$) to the adjacent minima (-0.40) is about $-5:2$. This is comparable with the corresponding displacements seen in figures 1–5 above.

This representation of the surface disturbance as a ripple with a sharp frequency

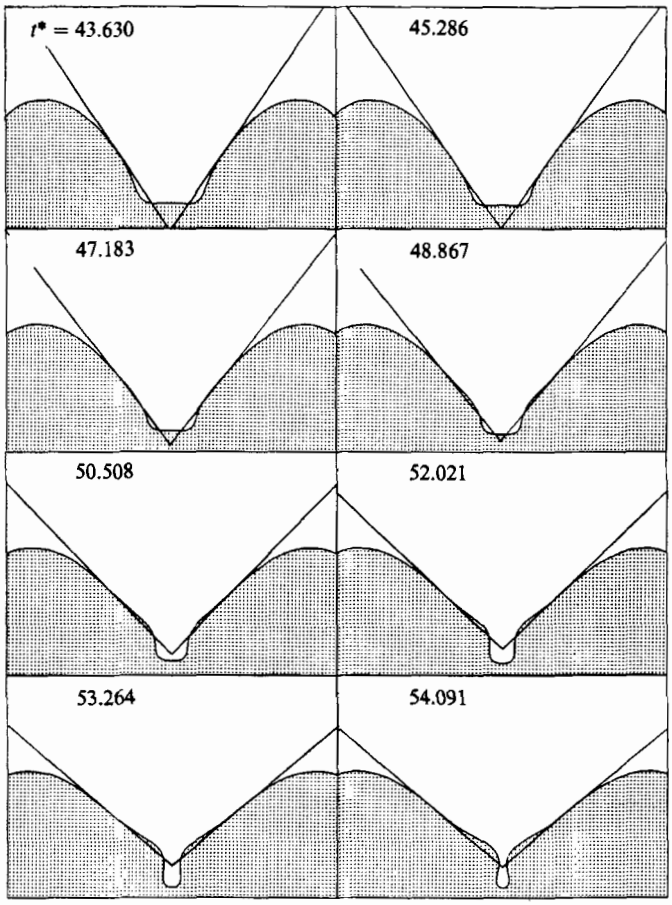

FIGURE 11. As figure 1, in the case of a typical raindrop: $R = 0.4375$ mm, $U = 3.565$ m/s.

σ and wavenumber k is of course an idealization. A closer representation would be as a pulse of finite bandwidth, that is

$$\eta(r, t, \bar{t}) = \int_{\Delta k} F(k, \bar{t})\, J_0(kr)\, \mathrm{e}^{\mathrm{i}\sigma t}\, \mathrm{d}k, \tag{6.2}$$

where $\bar{t}$ is a slow time and F is appreciably large only in a narrow range $\Delta k(\bar{t})$ of wavenumber. If, at time $t = 0$, η has a 'wave trough' at $r = 0$, i.e. a minimum, then a bubble may develop. If on the other hand η has a maximum there, an upwards jet will more probably emerge.

Note that nonlinearity will produce a qualitative difference between crests and troughs of the standing wave. Although nonlinear effects on *progressive* capillary waves are well-known (see Crapper 1957; Longuet-Higgins 1988) and result in a rounding of the wave crests relative to the wave troughs, the corresponding effects for standing waves have still to be determined (for a partial investigation, see Vanden-Broeck 1984). We may, however, expect that the surface slope in a standing capillary wave will become quite steep, even overhanging, before breaking occurs. Thus a nonlinear standing capillary wave at the point of breaking may correspond to a flow not unlike that in a fluid sink, as described above.

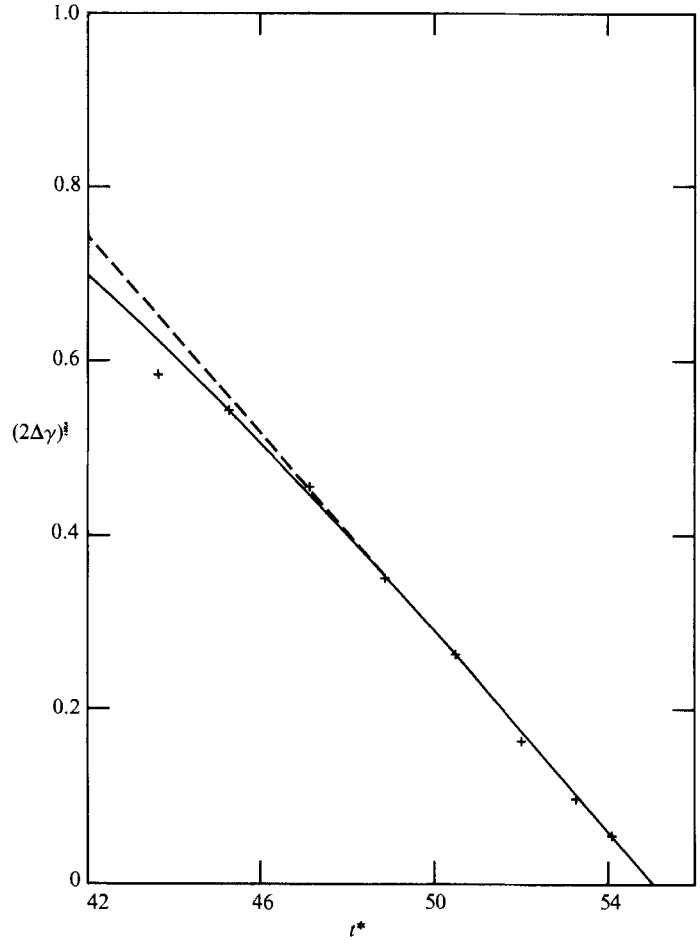

FIGURE 12. A plot of $(2\Delta\gamma)^{\frac{3}{2}}$ versus the dimensionless time t^* corresponding to figure 11.

7. Emission of sound

Typical pulses of sound emitted by the regular entrainment of bubbles are shown by Pumphrey *et al.* (1989, figure 3), or Pumphrey & Crum (1989, figure 15). The sound field has the form of a dipole, falling off with distance like r^{-1} in most directions (Pumphrey & Crum, figures 19 and 20). Such an acoustic field would be expected from a bubble oscillating as a monopole, but close to a pressure-release surface. At a distance $r = 1$ m vertically below a closed bubble, the initial amplitude of the acoustic pressure pulse as measured by Pumphrey & Crum (1989) is about 1 Pa, at a frequency of 8 kHz (their figure 19). At 14 kHz it is about 0.4 Pa.

Radial oscillations of a bubble may be stimulated in various ways:

1. By the closure pressure due to surface tension. The initial pressure is of order $2T/a$, where a is the mean bubble radius. Hence it will produce pressure oscillations of order $2T/r$ at a distance r from the bubble.

2. By 'shape oscillations' of the bubble, resulting from its initial distortion into a highly non-spherical shape. It has been shown that these give rise to a monopole radiation of sound having twice the fundamental frequency σ_n of the shape

oscillation. The pressure amplitude is of order $2\epsilon^2 T/r$, where ϵ is a distortion parameter, of order 1 (see Longuet-Higgins 1989*a*, *b*, *c*).

3. By the initial inwards momentum of the surrounding fluid at the time of closure. This will produce pressure oscillations with amplitude of order $\rho\omega\bar{u}a^2/r$, where ω is the radian frequency of the breathing mode and $\bar{u}$ the mean radial velocity at the surface of the bubble.

4. By spherical asymmetry in the velocity field. This will set up shape oscillations, and so generate second-order monopole pulsations in a similar way to (2).

With regard to (2) and (4) we note that near certain frequencies (calculated in Longuet-Higgins 1989*d*) the shape oscillations tend to resonate with the breathing-mode frequency ω, so as to produce an enhanced monopole emission of sound. Hence the estimates of the acoustic pressure may be increased by a factor 2 or more.

All of the above estimates are for bubbles in an unbounded fluid. When the bubble is close to a plane pressure-release surface, the far-field radiation will be in the form of a dipole, but decreased in amplitude by a factor δ of order $2h\omega/c$, where h is the distance of the bubble from the surface, ω is the radian frequency and c the speed of sound. For example, if we take $h = 3$ mm, $\omega/2\pi = 8$ kHz and $c = 1.5 \times 10^5$ cm/s, then δ is about 0.2.

If the surface is not perfectly plane, but has an axisymmetric indentation, as is observed, then it may be shown (see Longuet-Higgins 1989*d*; Oguz & Prosperetti 1989*b*) that the far field is still asymptotically a dipole, but that the amplitude is increased by a factor of order 3, if h now denotes the distance of the bubble below the lower point of the indentation. Hence δ may be taken to be about 0.6. With a higher frequency, say $\omega/2\pi = 14$ kHz, δ is about 1.

Consider first the bubble-closure mechanism (1). With $T = 74$ dyne/cm, and $r = 1$ m we find for the dipole moment rp:

$$r|p| = 2T = 0.15 \text{ N/m}. \tag{7.1}$$

This is less than the observed value by a factor of order 3.

Next, the initial-distortion mechanism (2) will produce an effect of magnitude ϵ^2 times that due to (1). Taking ϵ to be as great as 1, we see that the moment is at most of order

$$r|p| = 2\epsilon^2 T = 0.15 \text{ N/m}. \tag{7.2}$$

which is again less than the amplitude observed.

Consider now the mechanisms (3) and (4), which depend upon the initial velocity u near the bubble In this paper we have considered two velocity fields in particular.

(*a*) The hyperbolic flow (4.1). In this the radial velocity u at the bubble is given by

$$u = A(t)\, a(3\cos^2\theta - 1), \tag{7.3}$$

which is like a dipole. If we take account only of the part of the flow lying beneath the conical boundary $\theta = \theta_c$ then we find

$$\bar{u} = \tfrac{1}{2}A(t)\, a \int_{-1}^{3^{-\frac{1}{2}}} (3\mu^2 - 1)\, \mathrm{d}\mu = -\frac{1}{3^{\frac{3}{2}}} Aa. \tag{7.4}$$

Now from (4.7) and (4.11) we have, when $\tau \ll 1$,

$$A = -\frac{1}{(6t_0)^{\frac{2}{5}}} \frac{1}{t^{\frac{1}{5}}}. \tag{7.5}$$

Here t_0 denotes the timescale in (4.8) and (4.11), and t is the time at bubble closure.

We evaluate the above expressions for the raindrop example in figure 11. Comparing the timescales in figures 9 and 12, we see that

$$\frac{\mathrm{d}t^*}{\mathrm{d}\tau} = 25.5. \tag{7.6}$$

In figure 12 the timescale is given by

$$t_s = \frac{\mathrm{d}t}{\mathrm{d}t^*} = R/U = 0.123 \times 10^{-3}\ \mathrm{s}. \tag{7.7}$$

So from (4.11)

$$t_0 = \frac{3^{\frac{1}{2}}}{2}\frac{\mathrm{d}t}{\mathrm{d}\tau} = 2.72 \times 10^{-3}\ \mathrm{s}. \tag{7.8}$$

The instant t of bubble closure can be found by extrapolating the measured width W of the neck of the bubble; see figure 1. We find that W vanishes when $t^* = 54.32$. The time-difference between this and the intercept in figure 12 is

$$t = (54.32 - 55.02)\, t_s = -0.086 \times 10^{-3}\ \mathrm{s}. \tag{7.9}$$

From the observed frequency (14 kHz) we deduce a mean bubble radius a of about 0.02 cm. Altogether from (7.4) to (7.9) we find

$$|\bar{u}| = \frac{1}{3^{\frac{3}{4}}}\left(\frac{1}{6t_0}\right)^{\frac{2}{3}}\frac{a}{|t|^{\frac{1}{3}}} = 1.5\ \mathrm{cm/s}. \tag{7.10}$$

Hence

$$\rho\omega|u|a^2/r = 5.3\ \mathrm{Pa}. \tag{7.11}$$

This result depends only weakly on the assumed value of t in (7.10).

(*b*) The second flow considered earlier was the source (5.7) associated with the curvature of the cone. From (5.7) we have

$$r|p| = T\cot\gamma = \frac{T}{\sqrt{2}}, \tag{7.12}$$

that is

$$r|p| = 0.052\ \mathrm{N/m}, \tag{7.13}$$

which is an order of magnitude less than the contribution (7.11).

Since $t < 0$, it follows that the source (5.7) represents a flow inwards towards the centre. This is in the same sense as the resultant velocity $\bar{u}$ in the flow (*a*), so that the two effects tend to reinforce, not cancel each other. Together, they would appear to account largely for the observed pressure.

Because of the asymmetry of the flow (*a*), combined with the shape of the boundary, there will be a tendency for both flows (*a*) and (*b*) to excite shape oscillations of the bubble. However, since the distortion parameter ϵ can never exceed a certain value, of order 2, say, the sound emitted in this way cannot much exceed that given by equation (7.2). We note that there is some slight evidence in figure 22 from Pumphrey & Crum (1989) of increased emission at around the resonant frequencies 17, 27 and 47 kHz, estimated by Longuet-Higgins (1990).

8. Conclusions

We have shown that the conical profile often assumed by raindrop cavities may be associated with the simple flow (4.1) in which the time factor $A(t)$ is given by (4.8).

Such a flow develops a weak singularity near the time ($t = 0$) at which the vertex angle of the cone is 109.5°. The physical reason, as suggested in §4, is that the flow has to be forced through this configuration, and so there occurs a weak 'shock', when $A(t) \propto t^{-\frac{1}{3}}$. The time dependence of the flow near this instant is confirmed by observation.

Surface tension can be partly accounted for by introducing a time-dependent sink at the vertex of the cone: equation (5.7). This is made possible because in practice the vertex is surrounded by a small cavity in the free surface, which in turn is created by the convergence of a circular ripple towards the vertex.

The sound field from the bubble can be well accounted for by the inward radial momentum arising from these flows at the moment of bubble closure. The sound pulse generated by the closure itself appears to be somewhat smaller, as also is the pulse arising from the shape oscillations. The latter is probably only a small though perceptible part of the pulse produced by the initial inwards momentum, even at resonance. This may account for the slight indications of resonance seen in the data of Crum & Pumphrey (1989).

I am indebted to Professor A. Prosperetti and Dr H. Oguz for sending me a copy of their (1989) manuscript, from which some of the data in this paper were drawn, and to Dr Oguz for kindly supplying further details of his numerical calculations. The present work was supported under ONR Contract N00014-88C-0563.

REFERENCES

Crapper, G. D. 1957 An exact solution for progressive capillary waves of arbitrary amplitude. *J. Fluid Mech.* **96**, 417–445.

Longuet-Higgins, M. S. 1983 Bubbles, breaking waves and hyperbolic jets at a free surface. *J. Fluid Mech.* **127**, 103–121.

Longuet-Higgins, M. S. 1988 Limiting forms for capillary-gravity waves. *J. Fluid Mech.* **194**, 351–375.

Longuet-Higgins, M. S. 1989*a* Monopole emission of sound by asymmetric bubble oscillations. Part 1. Normal modes. *J. Fluid Mech.* **201**, 525–541.

Longuet-Higgins, M. S. 1989*b* Monopole emission of sound by asymmetric bubble oscillations. Part 2. An initial-value problem. *J. Fluid Mech.* **201**, 543–565.

Longuet-Higgins, M. S. 1989*c* Some integral theorems relating to the oscillations of bubbles. *J. Fluid Mech.* **204**, 159–166.

Longuet-Higgins, M. S. 1989*d* On the sound field due to an oscillating bubble near an indented free surface. *J. Fluid Mech.* (submitted).

Longuet-Higgins, M. S. 1990 Bubble noise spectra. *J. Acoust. Soc. Am.* **87**, 652–661.

Nystuen, J. A. 1986 Rainfall measurements using underwater ambient noise. *J. Acoust. Soc. Am.* **79**, 972–982.

Oguz, H. N. & Prosperetti, A. 1989*a* Bubble entrainment by the impact of drops on liquid surfaces (preprint, May 1989).

Oguz, H. N. & Prosperetti, A. 1989*b* Bubble oscillations in the vicinity of a nearby plane free surface. *J. Acoust. Soc. Am.* (submitted).

Prosperetti, A., Crum, L. A. & Pumphrey, H. C. 1989 The underwater noise of rain. *J. Geophys. Res.* **94**, 3255–3259.

Pumphrey, H. C. & Crum, L. A. 1988 Acoustic emissions associated with drop impacts. In *Sea Surface Sound* (ed. B. R. Kerman), pp. 463–483. Dordrecht, Reidel, 639 pp.

Pumphrey, H. C. & Crum, L. A. 1989 Sources of ambient noise in the ocean: an experimental investigation. *Univ. of Mississippi, Tech. Rep.* NCPA LC.011989, 96 pp.

PUMPHREY, H. C., CRUM, L. A. & BJORNO, L. 1989 Underwater sound produced by individual drop impacts and rainfall. *J. Acoust. Soc. Am.* **85**, 1518–1526.

SCRIMGER, J. A. 1985 Underwater noise caused by precipitation. *Nature* **318**, 647–649.

SCRIMGER, J. A., EVANS, D. J., MCBEAN, G. A., FARMER, D. M. & KERMAN, B. R. 1987 Underwater noise due to rain, hail and snow. *J. Acoust. Soc. Am.* **81**, 79–86.

SCRIMGER, J. A., EVANS, D. J. & YEE, W. 1989 Underwater noise due to rain – open ocean measurements. *J. Acoust. Soc. Am.* **85**, 726–731.

VANDEN-BROECK, J.-M. 1984 Nonlinear gravity–capillary standing waves in water of arbitrary uniform depth. *J. Fluid Mech.* **139**, 97–104.

WENZ, G. M. 1962 Acoustic ambient noise in the ocean: spectra and sources. *J. Acoust. Soc. Am.* **34**, 1936–1956.